Nonrigidity, delocalization, spatial confinement and electronic-vibrational spectroscopy of anthracene–helium clusters

Andreas Heidenreich, Uzi Even, and Joshua Jortner
School of Chemistry, Tel Aviv University, Ramat Aviv, 69978 Tel Aviv, Israel

(Received 29 January 2001; accepted 19 July 2001)

In this paper we present quantum mechanical calculations for the energetics, nuclear dynamics, spectral shifts, and vibrational level structure of anthracene·He_n ($n=1,2$) clusters in the ground (S_0) and in the first spin-allowed excited (S_1) electronic states. The anthracene–He potential in the S_0 state was described in terms of a sum of Lennard-Jones atom–atom potentials, while the potential in the S_1 state also included changes in dispersive energy and in repulsive interactions. Variational calculations were conducted for anthracene·He_1. For anthracene·He_2 we carried out configuration interaction calculations with the wave functions consisting of Hartree products, accounting for boson permutation symmetry. Extensive, anisotropic, one-dimensional spatial delocalization of the He atoms on the anthracene microsurface, which originates from large-scale confinement by the aromatic molecule, is exhibited, being further enhanced by repulsive interactions in the S_1 state and by the He–He repulsion. The anomalous size-dependence of the (red) spectral shifts for the $S_0 \rightarrow S_1$ electronic origin arises from mutually canceling dispersive and repulsive contributions which, together with the electronic-vibrational level structure, manifest quantum effects of anisotropic spatial delocalization, confinement and He–He interaction in nonrigid clusters. © *2001 American Institute of Physics.* [DOI: 10.1063/1.1401816]

I. INTRODUCTION

Cluster chemical physics focuses on the structure, isomer stereochemistry, electronic and nuclear level structure, spectroscopy, intrastate and interstate dynamics, electronic/nuclear response and chemical reactivity of large, finite systems.[1–3] Central issues in this research area pertain to the bridging between molecular, surface and condensed phase systems[4] and to the utilization of cluster size equations[4] as scaling laws[5] for the nuclear/electronic response of nanostructures. Notable recent developments in this broad interdisciplinary research area pertain to the exploration of quantum clusters, where the nuclear dynamics is dominated by quantum effects. Landmark examples involve $(^4He)_n$ ($n \geqslant 2$) and $(^3He)_n$ ($n \geqslant 25$) quantum clusters, which exhibit large zero-point energy motion, being liquid down to $T=0$ and manifest boson (for ^4He) or fermion (for ^3He) permutation symmetry.[6–19] Of considerable interest in this context is the phenomenon of superfluidity of boson $(^4He)_n$ finite clusters.[18–23] The structure and nuclear dynamics of large clusters of $(^4He)_n$ ($n \simeq 10^3-10^5$) were explored by the use of microscopic spectroscopic probes (e.g., dopant atoms or molecules[20–23]) or of a transport probe (e.g., an electron bubble[21]), which provided compelling experimental evidence for superfluidity at 0.4 K.[20–30] These experiments confirmed the conclusions from quantum path integral simulations of the collective excitations spectra and the superfluid fraction in smaller $(^4He)_n$ ($n=64$ and 128) clusters.[18]

A variety of molecules have been spectroscopically studied in $(^4He)_n$ clusters. The smaller species, e.g., OCS,[23,24] SF_6,[25] and linear monomers[26,27] studied by infrared spectroscopy provided information on the nature of local solvation in a superfluid.[28–30] The larger molecules, e.g., glyoxal,[21] interrogated by electronic spectroscopy provided evidence for a gap between the zero phonon line and the phonon sideband, due to the excitation of rotons in the superfluid cluster.[21] Large organic aromatic molecules, e.g., tetracene and pentacene in $(^4He)_n$ clusters[31] provide new avenues for the interrogation of local superfluid solvation on molecular microsurfaces. The electronic origin of tetracene in ^4He clusters at 0.4 K revealed splitting (~ 1 cm^{-1}) of the zero phonon line,[31] which cannot be attributed to a rotational structure, and was conjectured to arise from some kind of isomeric species.[20,31] These studies of molecular probes for superfluidity in ^4He droplets raise a renewed interest in aromatic-molecule·^4He clusters. Aromatic molecule rare-gas heteroclusters M·$(Rg)_n$ (M=benzene, anthracene, tetracene, pentacene and Rg≡Ne, Ar, Kr, Xe) have been extensively studied during the last two decades[1,32–35] for the elucidation of structural spectroscopic and dynamic facets of microscopic solvation phenomena, of the details of low-temperature rare-gas interactions with a graphite related microsurface, and of the structure and nature of structural isomers for an energy landscape characterized by multiple potentials minima. ^4He atoms bound to aromatic molecules,[36–51] constitute the extension of the M·Rg cluster family to the realm of nuclear quantum finite systems. Notable electronic-vibrational spectroscopic studies of benzene·He_n ($n=1,2$),[36,37] 2,3-dimethyl naphthalene·He,[48] and cyclopentadienyl·He radical[51] provided information on the cluster geometry, the van der Waals bond length, vibrational excitations and spectral shifts. The recent spectroscopic studies of Even and co-workers[49,50] on naphthalene·He_n, anthracene·He_n, and tetracene·He_n ($n=1-10$) in supersonic jets at $T=0.4$ K, provided extensive information on abnormal spectral shifts of the electronic ori-

gin of the $S_0 \rightarrow S_1$ transition and on the vibrational level structure in the S_1 electronic state of these clusters.

Aromatic molecule–He ($M \cdot He_n$) clusters are expected to exhibit some unique features due to nuclear quantum effects arising from large zero-point energy motion. These are manifested in the extensive delocalization of the He atoms on the aromatic microsurface and in the nonrigidity of the cluster donor to $T=0$. Concurrently, large-scale confinement effects will prevail, with the large-amplitude motion of the He atoms in $M \cdot He_n$ clusters being confined both vertically by the restoring force of the aromatic molecule and horizontally by the nuclear framework of the aromatic microsurface. Finally, the effects of boson (for ^{4}He) or fermion (for ^{3}He) permutation symmetry on energetics, nuclear dynamics, and collective excitations (for sufficiently large, low-temperature clusters) will be important. On the theoretical front, the delocalization of the He atom on the aromatic microsurface in excited vibrational states of 2,3-dimethyl naphthalene·He clusters was inferred by Bach *et al.*[48] from quantum mechanical calculations. Kwon and Whaley[52] conducted quantum path integral Monte Carlo simulations of benzene·He_{39} clusters over the temperature range 0.6–5 K, demonstrating the near complete localization of two helium atoms above and below the benzene ring. This classical-like spatial localization is consistent with the experimental spectroscopic determinations of the structure and bond length of benzene·He_n ($n=1,2$) (Refs. 36, 37) and of cyclopentadienyl·He (Ref. 51) clusters. These conclusions are in an apparent dichotomy with the notion of large-scale nuclear motion and nonrigidity of $M \cdot He_n$ clusters. However, in these He clusters, containing a single aromatic ring, the manifestations of horizontal (and vertical) confinement may be sufficient to attain nearly-rigid structures, whose spatial (averaged) configurations are amenable to study by the traditional methods of high-resolution spectroscopy. It thus appears that the manifestations of spatial delocalization should be explored in $M \cdot He_n$ clusters containing large aromatic molecules, e.g., anthracene and tetracene. We present quantum mechanical calculations for the energetics and nuclear dynamics of anthracene·He_n ($n=1,2$) clusters in the ground electronic state (S_0) and in the first spin-allowed electronically excited state (S_1). The geometries and topologies of the potential energy surfaces were constructed from pairwise interactions, which provide considerable insight into the nature of the nuclear-electronic level structure of these systems. Our studies of these large aromatic microsurfaces reveal extensive spatial anisotropic delocalization of He atoms at the ground vibrational level, both in the S_0 and S_1 electronic states, bringing up the notion of nonrigid $M \cdot He_n$ clusters. We shall account for the anomalous spectral shifts and for the vibrational level structure in the electronic-vibrational excitations of anthracene·He_n ($n=1-4$) clusters,[49,50] elucidating the implication of spatial delocalization, of horizontal large scale nuclear motion and of He–He interactions in these floppy quantum clusters.

II. METHODOLOGY

A. Potentials

For nonrigid clusters, e.g., anthracene·$(He)_n$, whose $(He)_n$ subpart is expected to be subjected to spatial delocalization even at 0 K, the symmetry of the nuclear Hamiltonian (within the framework of the Born–Oppenheimer separation of electronic and nuclear motion) is determined by the symmetry of the confining rigid nuclear framework of the aromatic molecule and by the permutation group of the indistinguishable He nuclei.

In our calculations of the energetics, spectral shifts and vibrational level structure of anthracene·He_1 and anthracene·He_2 clusters we kept the anthracene molecule rigid and spatially fixed. In the ground electronic state S_0 of anthracene, the anthracene-He potential V_0 was described in terms of a sum of atom–atom Lennard-Jones 6–12 potentials. We have utilized the potential parameters $\sigma_{C-He}=3.099$ Å, $\varepsilon_{C-He}=13.92\ cm^{-1}$, $\sigma_{H-He}=2.903$ Å, and $\varepsilon_{H-He}=5.761\ cm^{-1}$, which were taken from the study of Lim[53] on vibrational energy transfer in He–toluene. These potential parameters for the He–aromatic molecule interaction are more adequate than those based on the He–hydrogenated diamond interaction,[54–57] which we used in our preliminary calculations.[58] The anthracene·He potential V_1 in the S_1 electronically excited state of anthracene is given by

$$V_1 = V_0 + V_{DSS} + \Delta V_{LJ}, \tag{1}$$

where V_{DSS} is the change in the dispersive energy between the S_1 and S_0 electronic states, which was calculated by the dispersive spectral shift theory of Shalev and Jortner,[34,35] being given by

$$V_{DSS} = -\eta (e^2/2)\alpha_A \overline{F} \sum_{l=1}^{n} \sum_{\alpha,\beta} S_{\alpha\beta}^{(l)} G_{\alpha\beta}, \tag{2}$$

where $\alpha_A=0.204$ Å (Refs. 3 and 59) is the polarizability of the He atom, $\overline{F}=24.5$ eV its ionization energy, $S_{\alpha\beta}^{(l)}$ represents a geometric factor for the interaction of the C atoms α and β of the aromatic molecule with the lth He atom, while $G_{\alpha\beta}$ contains the contribution of the transition monopoles on the C atoms α and β of the aromatic molecule.[34,35] The scaling parameter η in Eq. (2) was chosen, in accord with previous calculations for heavy rare gas clusters,[34,35] as $\eta=0.6$. While for heavy rare gas–aromatic molecule clusters the dispersive contribution, Eq. (2), dominates the (red) spectral shift,[35] in the case of the anthracene·He_1 cluster the dispersive contribution to the (red) spectral shift $V_{DSS}=-11.0\ cm^{-1}$, estimated from Eq. (1), is by a numerical factor of ≈ 7 higher than the experimental spectral shift[49,50] of $\delta\nu_1=-1.6\ cm^{-1}$. This unusual behavior is due to the smaller C–He equilibrium distance, so that repulsive contributions can play a larger role in the excited state potential. We therefore introduced the term ΔV_{LJ} in Eq. (1), which represents the difference between the Lennard-Jones repulsive term of the S_1 and S_0 states,

$$\Delta V_{LJ} = 4\varepsilon \frac{\sigma_{ex}^{12} - \sigma^{12}}{R^{12}}, \tag{3}$$

with the excited state parameter σ_{ex}. We chose $\sigma_{ex}=1.0285\sigma$ for the carbon atoms in the 9, 10 positions. This parameter σ_{ex} (together with η) was taken to fit the experimental spectral shift of anthracene·He_1. For the He–He potential we used the *ab initio* potentials of Vos *et al.*[60] and of

TABLE I. Expansion coefficients g_i and Gaussian exponents γ_i of the Gaussian expansion of the He–He potential, Eq. (4).

No.	g_i /a.u.	γ_i /a.u.
1	1.98600	0.710680
2	0.25131	1.212015
3	-1.76275×10^{-4}	3.205385

Ceperley and Partridge[61] tabulated and reviewed by Aziz and Slaman.[62] While the potential values of Vos *et al.* (in Ref. 62 denoted as VVVVR) describe interatomic distances $R \geqslant 3.0$ a.u., the results of Ceperley and Partridge address the range $1.0\,\text{a.u.} \leqslant R \leqslant 3.0\,\text{a.u.}$ We employed a linear combination of three Gaussian functions,

$$V(R) = \sum_{i=1}^{3} g_i \exp(-R^2/2\gamma_i^2) \tag{4}$$

centered at $R=0$ to interpolate the tabulated potential values and to extrapolate them to interatomic distances of less than 1 a.u. Although several more sophisticated functional forms have been proposed[62] to fit the *ab initio* data, we chose the simpler linear combination of Gaussians with respect to an analytical solution of the two-particle integrals in a subsequent work. The expansion coefficients and Gaussian exponents were obtained by a least squares fit and are given in Table I. Figure 1 shows the fitted potential together with the *ab initio* data points. The fit to the *ab initio* data is excellent with deviations of 0.5 cm^{-1} at the potential minimum (where $V=-7.6\,\text{cm}^{-1}$), and of 1700 cm^{-1} at 1 a.u. (where $V=2.03\cdot10^5\,\text{cm}^{-1}$).

B. Variational calculations for anthracene·He$_1$

For anthracene·He_1 (An·He_1) we have performed variational calculations, using the following wave function $\Psi(x,y,z)$ of the helium atom in the potential well of the aromatic molecule,

$$\Psi(x,y,z) = \sum_{\mu=1}^{n} c_\mu \phi_\mu(x,y,z), \tag{5}$$

where c_μ are the linear expansion coefficients. x and y denote the short and the long molecular axis, respectively, with the center-of-mass of the anthracene molecule as the origin of the coordinate system. At present, in all calculations of An·He_1 and An·He_2, the coordinate z perpendicular to the molecular plane is restricted to values $\geqslant 0$. As a consequence of the limitation $z \geqslant 0$, the point group of the An·He_n system is C_{2v}. The three-dimensional (3D) basis functions $\phi_\mu(x,y,z)$ are taken as products of one-dimensional (1D) functions,

$$\phi_\mu(x,y,z) = \phi_{\mu x}(x)\,\phi_{\mu y}(y)\,\phi_{\mu z}(z). \tag{6}$$

The 1D functions $\phi_{\mu x}(x)$, $\phi_{\mu y}(y)$, and $\phi_{\mu z}(z)$ are the numerical solutions of the Schrödinger equation for one-dimensional cuts $V_{y=0,z=\text{opt}}(x)$, $V_{x=0,z=\text{opt}}(y)$, and $V_{x=0,y=0}(z)$ of the intermolecular potential $V_0(x,y,z)$ of the ground electronic state of anthracene. Specifically, the cuts $V(x)$ and $V(y)$ were taken for fixed values of $y=0$ and $x=0$, respectively, and the z coordinate was optimized with respect to the minimum potential energy. The cut $V(z)$ was taken at $x=0$, $y=0$. Figure 2 shows the 1D cuts $V(x)$, $V(y)$, and $V(z)$ of the anthracene electronic ground state potential together with the lowest 1D eigenfunctions and their eigenvalues. Since the 1D functions are orthonormal, so are the 3D product functions, Eq. (6), which also form an orthonormal basis set. Each 3D basis function is completely characterized by the triple (μ_x,μ_y,μ_z) 1D quantum numbers. As indicated in Fig. 2(c) the 1D basis functions were considered only for $z>0$, i.e., tunneling or side crossing was disregarded in the linear variational calculations. The kinetic and potential energy integrals were calculated numerically.

Our variational calculations for An·He_1 involve 165 3D basis functions, spanning all possible triples (μ_x,μ_y,μ_z) for $0\leqslant\mu_x\leqslant4$, $0\leqslant\mu_y\leqslant10$, and $0\leqslant\mu_z\leqslant2$. This basis set, derived from the 1D cuts of the ground electronic state potential $V_0(x,y,z)$, also served in the variational calculations of the S_1 state with the potential given by Eq. (1).

More extensive calculations were also conducted. Test calculations for anthracene·He_1 involving both sides of the aromatic molecule and large basis sets of up to 1200 3D (Lowdin orthogonalized) basis functions, consisting of our original basis set and additional Gaussian functions, were

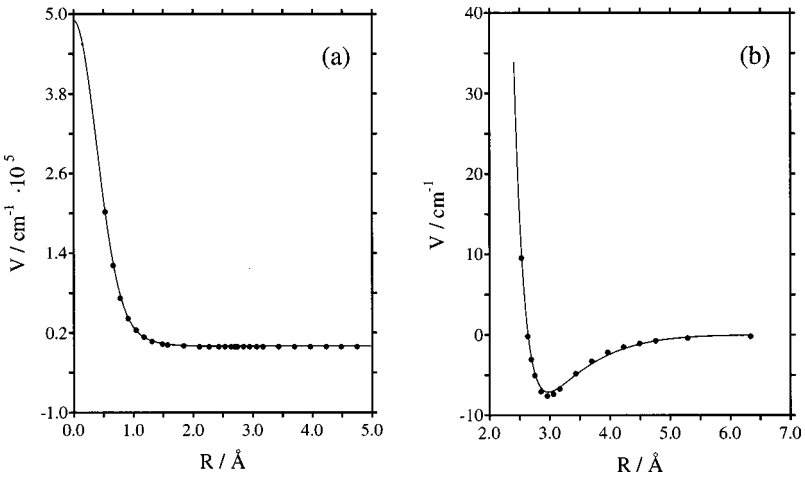

FIG. 1. The He–He potential. (a) The entire potential curve. (b) A magnified part at the minimum of the potential curve. The data points represent the tabulated *ab initio* data (Refs. 60–62) and the solid curves represent the Gaussian fit, Eq. (4).

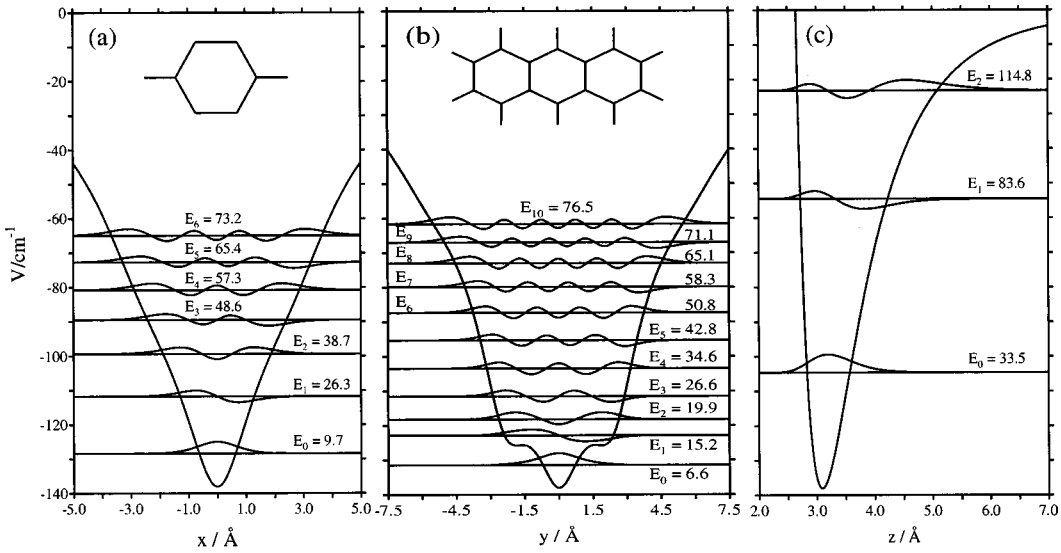

FIG. 2. One-dimensional cuts of the anthracene–helium ground electronic state potential along the *x*, *y*, and *z* axes. For the cut (a) along the *x* axis, *y* was set to 0 and the *z* coordinate was optimized according to the minimum potential energy for the given *x*, *y* pair. Cut (b) along the *y* axis was taken at $x=0$ with the *z* coordinate optimized. The 1D cut (c) along the *z* axis was obtained for $x=0$ and $y=0$. The 1D eigenfunctions, which served as basis functions in the subsequent variational calculations, are included in the diagrams; their eigenvalues E_I are given relative to the minimum potential energy -138.1 cm^{-1}. To compare the spatial extension of the 1D wave functions in the *x* and *y* directions with the size of the molecule, the anthracene molecule (b) and its central ring (a) have been included at the same scale.

conducted. These calculations led to similar (within 1 cm^{-1}) ground state energies, while the spectral shift, the transition energies and the Franck–Condon factors are relatively little effected. Side crossing or tunneling was not found to have a notable influence on transition energies in the energy range of interest ($\approx$40 cm^{-1}), as the addition of basis functions located in the molecular plane, but beyond the hydrogen atoms, showed.

C. Configuration interaction calculations for anthracene·He$_2$

For the An·He$_2$ cluster we have performed configuration interaction (CI) calculations. The nuclear wave function was taken as a linear combination of symmetrized Hartree products ("permanents") $\Delta_a(1,2)$, so that

$$\Psi(1,2)=\sum_a (c_a\Delta_a(1,2)) \tag{7}$$

with 1 and 2 denoting the Cartesian coordinates of helium atoms 1 and 2,

$$\Delta_a(1,2)=\frac{1}{\sqrt{N_a}}\sum_{P=1}^{2!}\left(\hat{P}\prod_\mu(\phi_\mu)\right), \tag{8}$$

where N_a is the normalization integral of the permanent and $\hat{P}$ is the permutation operator. Each permanent is built up by the 3D basis functions ϕ_μ defined in Sec. II B and is spin (0) and symmetry adapted. For a two-boson system there are two types of permanents, denoted here as type 1, $\Delta_1(\mu,\mu)$, or type 2, $\Delta_2(\mu,\nu)$, respectively, which are constructed either from identical 3D functions, ϕ_μ, or from different 3D functions ϕ_μ and ϕ_ν,

$$\Delta_1(\mu,\mu)=\phi_\mu(1)\phi_\mu(2), \tag{9}$$

$$\Delta_2(\mu,\nu)=\frac{1}{\sqrt{2}}(\phi_\mu(1)\phi_\nu(2)+\phi_\nu(1)\phi_\mu(2)). \tag{10}$$

The notation of Eqs. (9) and (10) stresses the occupation of 3D basis functions, rather than the dependence on the atomic coordinates of helium atoms 1 and 2, cf. Eqs. (7) and (8). The Hamiltonian of the An·He$_2$ system is

$$\hat{H}=\hat{h}(1)+\hat{h}(2)+\hat{g}(1,2), \tag{11}$$

where $\hat{h}(1)$ and $\hat{h}(2)$ are the one-particle operators, which consist of the kinetic energy operators of the helium atoms and the potential energy operator of the helium in the field of the aromatic molecule. $\hat{g}(1,2)$ is the two-particle potential energy operator between the two helium atoms, for which the superposition of Gaussians, Eq. (4), was taken (Sec. II A). The matrix elements of the Hamiltonian in the basis of the permanents, Eq. (8), are

$$\langle\Delta_1(\mu,\mu)|\hat{H}|\Delta_1'(\nu,\nu)\rangle=2h_{\mu\nu}\delta_{\mu\nu}+(\mu\nu|\mu\nu), \tag{12}$$

$$\begin{aligned}\langle\Delta_2(\mu,\nu)|\hat{H}|\Delta_2'(\lambda,\sigma)\rangle&=h_{\mu\lambda}\delta_{\nu\sigma}+h_{\mu\sigma}\delta_{\nu\lambda}+h_{\nu\lambda}\delta_{\mu\sigma}+h_{\nu\sigma}\delta_{\mu\lambda}\\&\quad+(\mu\lambda|\nu\sigma)+(\mu\sigma|\nu\lambda),\end{aligned} \tag{13}$$

$$\langle\Delta_1(\mu,\mu)|\hat{H}|\Delta_2(\lambda,\sigma)\rangle=\sqrt{2}[h_{\mu\lambda}\delta_{\mu\sigma}+h_{\mu\sigma}\delta_{\mu\lambda}+(\mu\lambda|\mu\sigma)], \tag{14}$$

with

$$h_{\mu\nu}=\int d\tau_1\phi_\mu(1)\hat{h}(1)\phi_\nu(1) \tag{15}$$

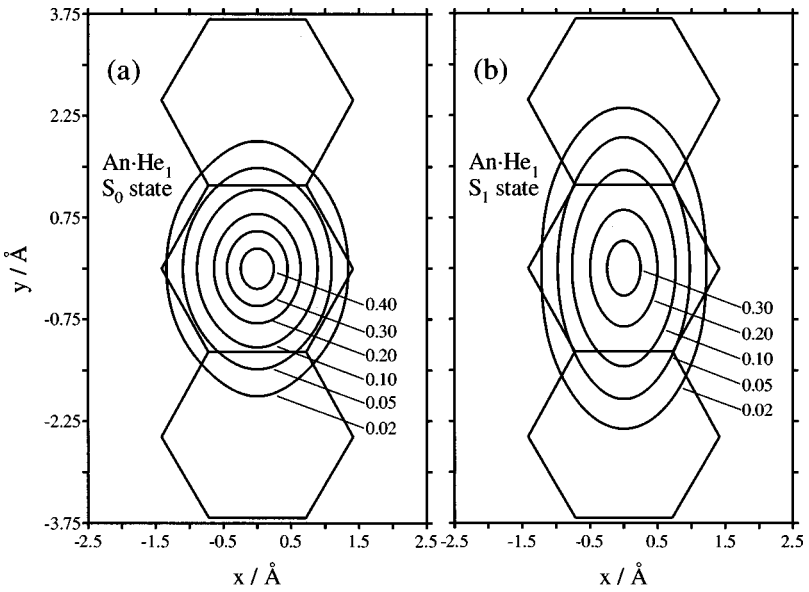

FIG. 3. Contour plots of the probability density of the helium atom on the anthracene molecular surface for the vibrational ground states of anthracene·He_1, (a) for the S_0 and (b) for the S_1 state.

and

$$(\mu\nu|\lambda\sigma)=\int d\tau_1\int d\tau_2\phi_\mu(1)\phi_\nu(1)\hat{g}(1,2)\times\phi_\lambda(2)\phi_\sigma(2), \tag{16}$$

where τ_1 and τ_2 denote the entire three-dimensional definition range of helium atoms 1 and 2, respectively.

All the one- and two-particle integrals were solved numerically, exploiting the C_{2v} symmetry of the confining one-sided, rigid anthracene nuclear framework. The large number of two-particle integrals requires that the numerical solution is very efficient. The two-particle integrals are sixfold integrals, ruling out a numerical solution at first glance. However, the two-body potential $g(1,2)$ depends on a coordinate difference, so that the sixfold integrals can be factorized into a threefold integral and three single integrals,

$$\begin{aligned}&\int_{-\infty}^{\infty}dx_1\int_{-\infty}^{\infty}dy_1\int_{-\infty}^{\infty}dz_1\int_{-\infty}^{\infty}dx_2\int_{-\infty}^{\infty}dy_2\int_{-\infty}^{\infty}dz_2\phi_{\mu x}(x_1)\\&\times\phi_{\mu y}(y_1)\phi_{\mu z}(z_1)\phi_{\nu x}(x_1)\phi_{\nu y}(y_1)\phi_{\nu z}(z_1)\\&\times g(x_2-x_1,y_2-y_1,z_2-z_1)\phi_{\lambda x}(x_2)\phi_{\lambda y}(y_2)\\&\times\phi_{\lambda z}(z_2)\phi_{\sigma x}(x_2)\phi_{\sigma y}(y_2)\phi_{\sigma z}(z_2)\\&=\int_{-\infty}^{\infty}dx\int_{-\infty}^{\infty}dy\int_{-\infty}^{\infty}dz g(x,y,z)F_x(x)F_y(y)F_z(z),\end{aligned} \tag{17}$$

with $x=x_2-x_1$, $y=y_2-y_1$, $z=z_2-z_1$, and the cross-correlation functions $F_x(x)$, $F_y(y)$, $F_z(z)$, e.g.,

$$F_x(x)=\int_{-\infty}^{\infty}dx_1\phi_{\mu x}(x_1)\phi_{\nu x}(x_1)\times\phi_{\lambda x}(x_1+x)\phi_{\sigma x}(x_1+x). \tag{18}$$

In order to reduce the computational demand of each three-dimensional integral, Eq. (17), the integration limit was truncated as much as possible, making use of the fact that $g(x,y,z)$ acts as a damping factor of the products of the three cross-correlation functions. For the present calculation the integration was limited from -2.55 Å to $+2.55$ Å. This truncation of the integration limit is justified by the fact that the repulsive part of the He–He potential gives the dominant contribution to the He–He integrals, and that the attractive He–He interaction is weak compared to the anthracene–He interactions.

Our CI calculation involved 165 3D basis functions, spanning the 1D quantum numbers $0\leqslant\mu_x\leqslant4$, $0\leqslant\mu_y\leqslant10$, and $0\leqslant\mu_z\leqslant2$. From these 3D basis functions all possible permanents have been generated, resulting in $\approx$3600 permanents and $\approx2.3\cdot10^7$ He–He integrals for each symmetry type of the point group C_{2v}.

III. RESULTS AND DISCUSSION

A. Spatial delocalization of He atoms

For the anthracene·He_1 $(1|0)$ configuration, the nuclear wave function of the vibrational ground state consists almost exclusively of ϕ_{000} (coefficient 0.99 and 0.95 for the S_0 and S_1 electronic states, respectively). A cursory examination of the three 1D components of this ground state vibrational wave function (Fig. 2) reveals that the energy of the helium atom in the long axis y direction is located below the double minimum of the two outer rings and no tunneling splitting is exhibited for the motion along the long (y) in plane axis. Figure 3 shows the probability density $P(x,y)$ of the helium atom on the anthracene surface for the $(1|0)$ configuration,

$$P(x,y)=\int_0^{\infty}dz\Psi^2(x,y,z). \tag{19}$$

While in the ground vibrational level of the S_0 state the helium atom is mainly located over the central ring, in the ground vibrational level of the S_1 state the density is shifted towards the outer rings. The probability density can be characterized by its standard deviations $\langle\Delta x^2\rangle^{1/2}$, $\langle\Delta y^2\rangle^{1/2}$, and $\langle\Delta z^2\rangle^{1/2}$ in the x, y, and z directions, respectively. The stan-

TABLE II. Anisotropic spatial delocalization of He atoms on anthracene in the ground vibrational state of the S_0 and S_1 electronic states.

Standard deviation (Å)	Anthracene·He$_1$		Anthracene·He$_2$	
	S_0	S_1	S_0	S_1
$\langle\Delta x^2\rangle^{1/2}$	0.55	0.54	0.60	0.57
$\langle\Delta y^2\rangle^{1/2}$	0.75	0.99	1.91	1.96
$\langle\Delta z^2\rangle^{1/2}$	0.29	0.30	0.31	0.31
First moment $\langle z\rangle$ (Å)	3.33	3.36	3.35	3.34

dard deviations for the S_0 and S_1 states are displayed in Table II. These parameters can be taken as a measure of nonrigidity in the ground vibrational state of S_0 and S_1. The He atom is grossly delocalized (at $T=0$) in both the S_0 and the S_1 states. The horizontal spatial delocalization along the long y axis is especially large (Table II). We also note the considerable spread of the density in the S_1 state relative to the S_0 state in the y direction, while remaining unchanged in the x and z directions. The delocalization in the y direction across the central ring of the anthracene molecule is large (Fig. 3), increasing from $\langle\Delta y^2\rangle^{1/2}=0.75$ Å in S_0 to $\langle\Delta y^2\rangle^{1/2}=0.99$ Å in S_1 (Table II). The enhanced spread of the vibrational ground state density in the S_1 state along the y axis can be readily understood from a contour plot of the difference potential $\Delta V=V_1-V_0$, i.e., a contour plot of the spectral shift, Fig. 4. Due to the enhanced repulsion at the 9, 10 carbon atoms, the contour plot shows positive potential differences in the central ring, causing a decrease of the probability density in this region.

For the An·He$_2$ one-sided $(2|0)$ configuration extensive mixings of the permanents are exhibited for the ground vibrational levels of the S_0 and S_1 states, with the major contributions to the wave function being $0.45\Delta(\phi_{0,0,0}\phi_{0,2,0}) - 0.52\Delta(\phi_{0,1,0}\phi_{0,1,0}) - 0.40\Delta(\phi_{0,1,0}\phi_{0,3,0}) + 0.46\Delta(\phi_{0,2,0}\phi_{0,2,0})$ for the S_0 state and $0.41\Delta(\phi_{0,0,0}\phi_{0,2,0}) - 0.52\Delta(\phi_{0,1,0}\phi_{0,1,0}) - 0.44\Delta(\phi_{0,1,0}\phi_{0,3,0}) + 0.51\Delta(\phi_{0,2,0}\phi_{0,2,0})$ for the S_1 state. The coefficient of the $\Delta(\phi_{0,0,0}\phi_{0,0,0})$ configuration in the vibrational ground state wave function for both the S_0 and the S_1 state is small (≈ 0.1) due to the large He–He repulsion. Figure 5 shows the one-particle density $P(x,y)$ for the $(2|0)$ configuration,

$$P(x,y)=P(x_1,y_1)=2\int_0^\infty dz_1\int_{-\infty}^\infty dx_2\int_{-\infty}^\infty dy_2\int_0^\infty dz_2 \times\Psi^2(x_1,y_1,z_1x_2,y_2,z_2). \quad (20)$$

Due to the He–He repulsion, $P(x,y)$ is delocalized over the three aromatic rings in the y direction already in the ground electronic state. The spatial delocalization is even slightly enhanced in the S_1 state. The standard deviations in the x, y, and z directions are summarized in Table II.

The one-particle densities allow for the observation and quantification of extensive anisotropic spatial delocalization of the He atoms on the anthracene microsurface in the ground vibrational state of anthracene·He$_n$ $(n=1,2)$ clusters, both in the S_0 and S_1 electronic states. The spatial delocalization of both one or two He atoms along the perpendicular z axis, i.e., $\langle\Delta z^2\rangle^{1/2}=0.3$ Å, is quite substantial, but is confined by the strong restoring force of the aromatic frame. Similarly, the spatial delocalization for both the $(1|0)$ and $(2|0)$ configurations along the short horizontal x axis, i.e., $\langle\Delta x^2\rangle^{1/2}=0.54-0.60$ Å, is confined by the horizontal nuclear framework of a single aromatic ring. We also note that the He–He repulsion in the $(2|0)$ configuration does not markedly modify the spatial delocalization across the z and x axes in large aromatic molecules, which are dominated by the vertical (z) and horizontal (x) confinement. The physical situation is drastically different for the large scale horizontal motion along the long y axis on the microsurface of large aromatics, which reveals a considerable sensitivity to the repulsive interactions with the large aromatic frame for

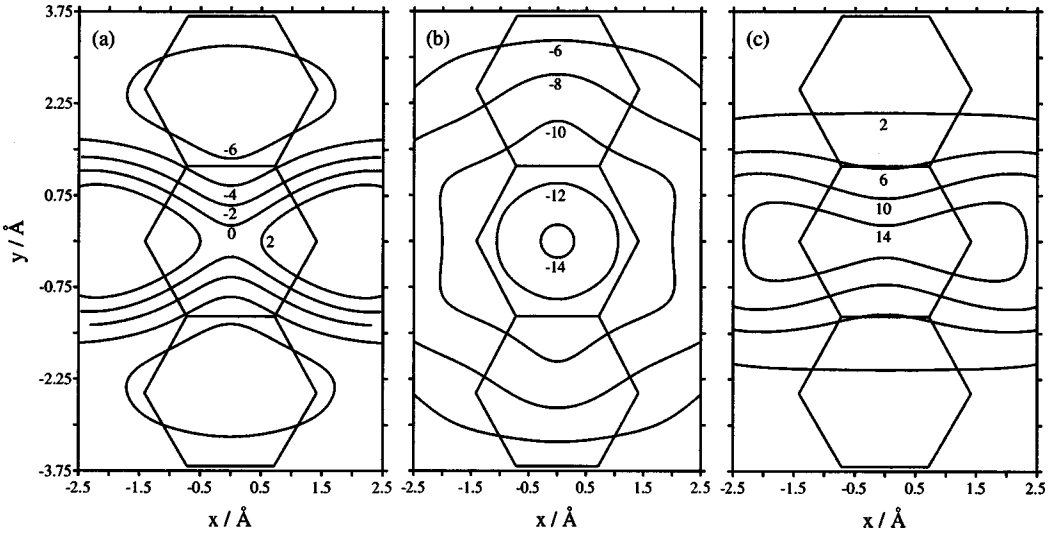

FIG. 4. The contour plot of the difference potential $\Delta V=V_1-V_0$ on the anthracene molecular surface. For each point in the x, y plane the z coordinate was optimized according to the minimum potential energy at that point. (a) The total difference potential, (b) the dispersive, and (c) the repulsive contributions to the difference potential.

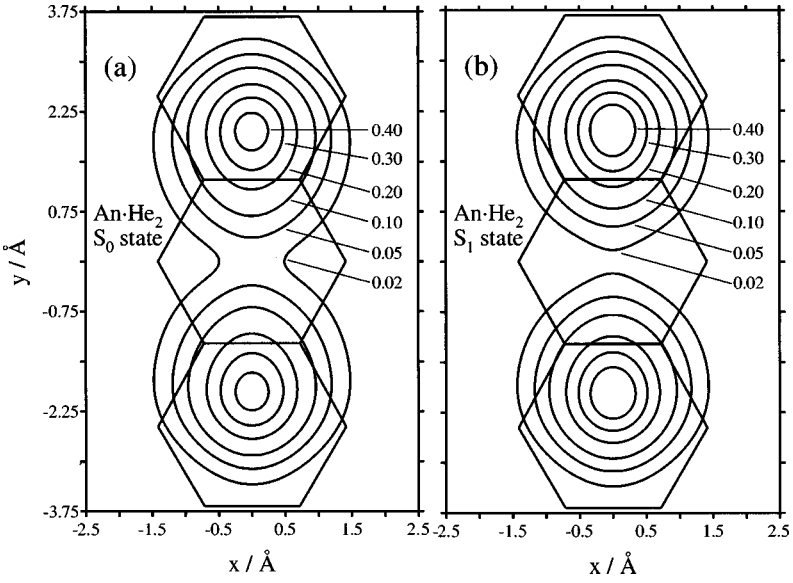

FIG. 5. Contour plots of the one-particle densities of the helium atom on the anthracene molecular surface for the vibrational ground states of anthracene·He_2, (a) for the S_0 state and (b) for the S_1 state.

An·He_1, discussed above, and to the effects of He–He repulsion for An·He_2. The one-particle probability density along the y axis for An·He_2 (Fig. 5) reveals delocalization across the two terminal aromatic rings of the anthracene molecule. The pushing of the delocalized probability density from the central ring for An·He_1 to the two center rings for An·He_2 is induced by the strong He–He repulsive interactions in An·He_2. This delocalization along the long y axis is described by the second central moments $\langle \Delta y^2 \rangle^{1/2} = 1.91$ Å for the S_0 state and $\langle \Delta y^2 \rangle^{1/2} = 1.96$ Å for the S_1 state. The small increase of $\langle \Delta y^2 \rangle^{1/2}$ in the electronically excited state of An·He_2 manifests the dominating role of the He–He repulsions, which overwhelm the change of the repulsive interaction with the large aromatic frame in the S_1 state.

B. Spectral shifts

Even *et al.* observed[49,50] an anomalous size dependence of the spectral shifts of the $S_0 \rightarrow S_1$ electronic origin of anthracene·He_n ($n=1-4$) clusters, which correspond to the lowest-energy excitation of each mass-selected cluster (Fig. 6) are to the red, manifesting the dominance of dispersive interactions for $\delta\nu$. The $n=1$ cluster reveals a low value of $\delta\nu_1 = -1.6\,\mathrm{cm}^{-1}$, which was attributed to the one-sided (1|0) structure.[49] The configurations of larger clusters ($n=2-4$) were inferred[49] on the basis of additivity rules for spectral shifts.[49] The $n=2$ cluster, with $\delta\nu_2 = -3.2\,\mathrm{cm}^{-1}$, was assigned[49] to the two-sided (1|1) cluster in view of the additivity relation $\delta\nu_2 = 2\,\delta\nu_1$. The large jump of $\delta\nu_3 = -12.6\,\mathrm{cm}^{-1}$ was attributed[49] to the (2|1) structure for anthracene·He_3. The experimental spectral shift $\delta\nu_4 = -21.9\,\mathrm{cm}^{-1}$ for the $n=4$ cluster was assigned[49] to the two-sided (2|2) structure, with the experimental value of $\delta\nu_4$ being in accord with the estimate $\delta\nu(2|2) = 2\,\delta\nu(2|0) = -22.0\,\mathrm{cm}^{-1}$. The anthracene·$He_n$ clusters reveal an irregular pattern of the spectral shift, with an abrupt jump of $\delta\nu_n$ versus n at $n=3$ (Fig. 6), which is manifested by the surprisingly large enhancement of $\delta\nu$ for $\delta\nu(2|0)$ relative to the (1|1) configuration. This behavior is in marked difference with spectral shifts of aromatic molecules with heavy rare gases (Ar, Kr, Xe), where the size dependence of $\delta\nu$ is gradual and isomer specificity of $\delta\nu$ is small (10%–20%).[35] We shall now show that this dramatic large difference between the spectral shift for two-sided and one-sided structures of anthracene·He_2 originates from the large amplitude quantum motion of two He atoms on the microsurface of anthracene, which will change the balance between the dispersive and repulsive contributions to the spectral shift.

The vibrational states of the (1|0) and (2|0) cluster configurations are classified according to the point symmetry of the (one-sided) anthracene microsurface. The vibrational level structures in the S_0 and S_1 states are presented in Fig. 7. The spectral shifts for the electronic origin of the $S_0 \rightarrow S_1$ transition were calculated from the difference of the

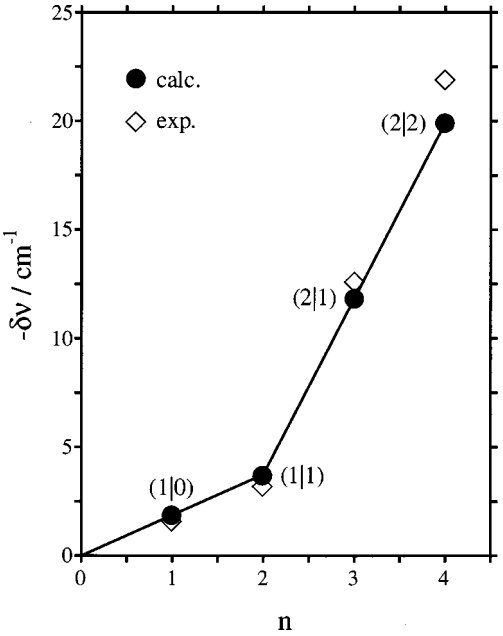

FIG. 6. A comparison of the calculated (present work) and the experimental (Ref. 49) red spectral shifts for anthracene·He_n, $n=1-4$. The calculated spectral shifts for $n>1$ clusters were obtained as sums of the spectral shifts of the (1|0) and of the (2|0) configurations, using additivity rules.

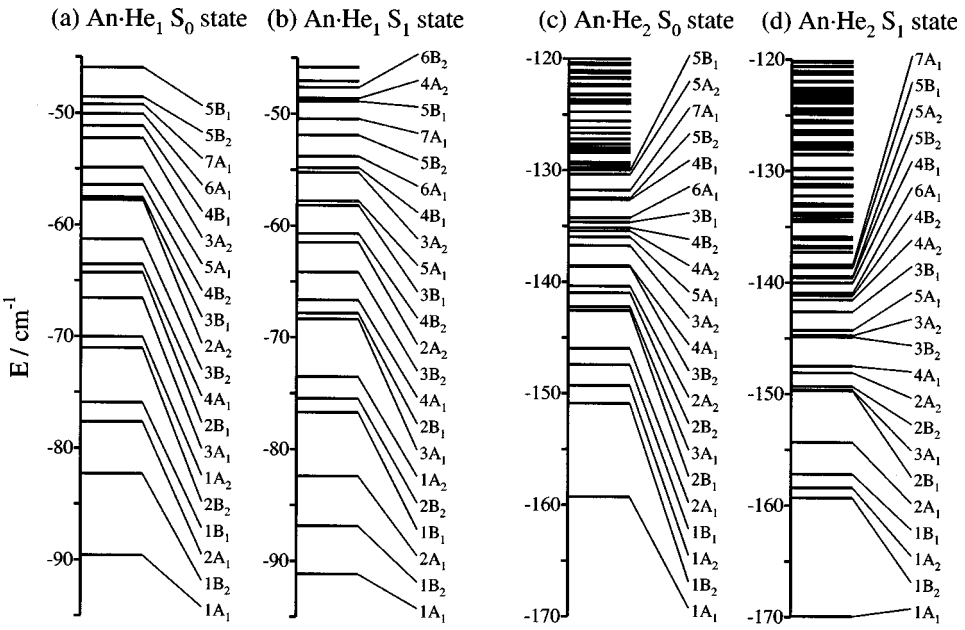

FIG. 7. Vibrational level diagrams for the $(1|0)$ and for the $(2|0)$ cluster configuration in the S_0 and in the S_1 electronic state. The vibrational states are classified according to the C_{2v} point symmetry of the (one-sided) anthracene microsurface, with the symmetry type B_2 denoting wave functions being antisymmetric with respect to the *xz* plane.

$1A_1$ state eigenvalues in the S_1 and S_0 electronic states (Fig. 7). The spectral shift $\delta\nu(1|0)$ for the $n=1$ $(1|0)$ configuration is calculated as $\delta\nu(1|0)=-1.6\,\mathrm{cm}^{-1}$ and is presented in Fig. 6. This small spectral shift constitutes near-cancellation between dispersive, attractive (red) and repulsive (blue) contributions.

The spectral shift can also be approximately estimated from the first moment of the difference potential ΔV (Fig. 4), being given by the expectation value of ΔV for the one-particle (nuclear) density $P(x,y,z)$ of the vibrational ground state of S_0,

$$\delta\nu \approx \int_{-\infty}^{\infty} dx \int_{-\infty}^{\infty} dy \int_{0}^{\infty} dz P(x,y,z)\Delta V(z,y,z). \qquad (21)$$

Knowing the one-particle density, this approximate expression can provide information concerning parts of the molecule that contribute to the spectral shift, and it provided us with a valuable tool for adjusting the excited state potential V_1, presented in Sec. II A and utilized herein. The one-particle density for the $(1|0)$ and $(2|0)$ configurations, which are markedly delocalized in the *y* direction, caused the drastic increase of the red spectral shift, calculated in Eq. (20), from -1.6 cm^{-1} for the $(1|0)$ configuration to the value of -11 cm^{-1} for the $(2|0)$ configuration. The marked enhancement of the red spectral shift reflects on the large increase of the anisotropic delocalization due to He–He repulsion, which drives the density towards outer regions of negative ΔV values (Fig. 4) in the $(2|0)$ configuration.

The calculated spectral shift for the $(2|0)$ cluster, obtained from the difference of the $1A_1$ state eigenvalues in S_1 and S_0, is $\delta\nu=-10.7\,\mathrm{cm}^{-1}$, being higher by a numerical factor of ~ 7 than the corresponding spectral shift for the $(1|0)$ cluster. Invoking the additivity rules for anthracene·He_n $(n=1-4)$ we used our theoretical results for the $(1|0)$ and $(2|0)$ configurations to calculate the spectral shift for the $n=2(1|1)$, $n=3(1|2)$, and $n=4(2|2)$ clusters. The calculated spectral shifts (Fig. 6) account well for the abrupt jump in $\delta\nu$ versus *n* between $n=2$ and $n=3$, originating from the enhancement of dispersive interactions due to large amplitude parallel motion of the two He atoms located on one side of the microsurface of anthracene.

C. Electronic-vibrational level structure

The calculated vibrational level structures of the $(1|0)$ and $(2|0)$ configurations (Fig. 7) provide information on electronic-vibrational spectroscopy of anthracene·He_n clusters $(n=1-4)$. The vibrational level structure in the S_0 state of anthracene·He_1 (Fig. 7) reveals that the lowest vibrational excitations are $7.3\,\mathrm{cm}^{-1}$ $(1B_2)$ and $12.0\,\mathrm{cm}^{-1}(2A_1)$, respectively, so that their thermal population is negligible under the experimental conditions of Even *et al.* $(T=0.4\,\mathrm{K})$.[49,50] Accordingly, only $S_0(1A_1)\rightarrow S_1(nA_1)$ electronic-vibrational transitions, which involve the $1A_1$ state as the initial state, contribute to the spectra. We calculated the transition energies and the Franck–Condon vibrational overlap factors for the allowed $S_0(1A_1)\rightarrow S_1(nA_1)$ electronic-vibrational excitations of the $(1|0)$ and $(2|0)$ configurations. These data allowed us to obtain the anthracene·He_n $(n=1-4)$ vibronic spectra by again invoking the additivity rules. The calculated $n=1$ cluster spectrum corresponds to $(1|0)$, the calculated $n=2$ cluster spectrum is taken as that for $(1|1)[=(1|0)+(0|1)]$, the calculated $n=3$ cluster spectrum was chosen as that for $(2|1)[=(2|0)+(0|1)]$, while the $n=4$ calculated spectrum was attributed to $(2|2)[=(2|0)+(0|2)]$. The comparison between the calculated stick spectra and the experimental spectra[49,50] is presented in Fig. 8. The prominent calculated vibrational excitations in the S_1 state origi-

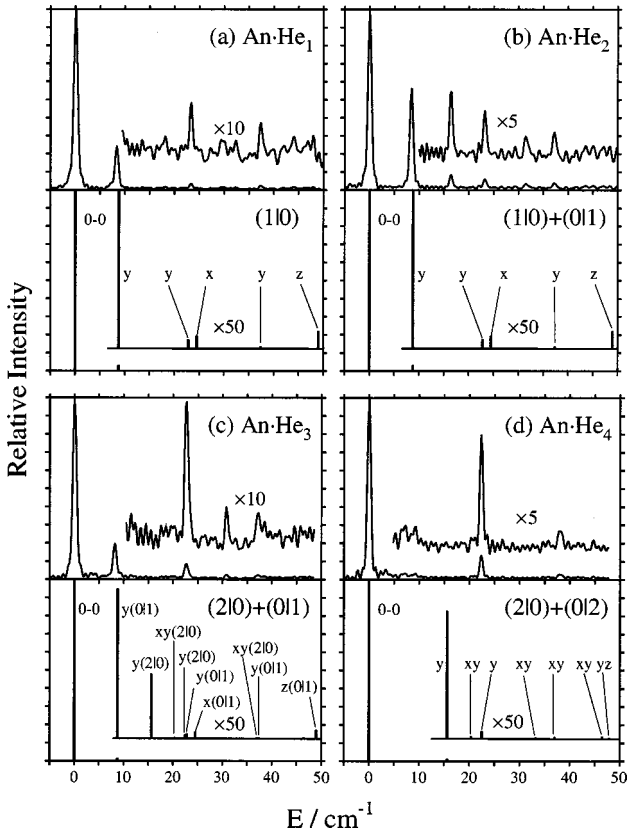

FIG. 8. A comparison of experimental vs calculated spectra. The calculated vibronic lines (lower panels) are represented as sticks whose length is proportional to the Franck–Condon factors. According to the additivity rules, the calculated spectrum of the anthracene·He_2 cluster (b) is compared with the theoretical spectrum of the (1|0) isomer, of the anthracene·He_3 cluster (c) by a superposition of the (1|0) and of the (2|0) subspectra, and of the anthracene·He_4 cluster (d) by the theoretical spectrum of the (2|0) isomer. The nature of the vibronic transitions is labeled by *x*, *y*, and *z*. In panels a and b the magnified calculated intensities of the first [*y*] transition exceed the intensity range of the graphs.

nate from major contributions of $\phi_{\mu x,0,0}[x]$, $\phi_{0,\mu y,0}[y]$, $\phi_{\mu x,\mu y,0}[xy]$, and of $\phi_{0,0,\mu z}[z]$, $\phi_{0,\mu y,\mu z}[yz]$, where $[x]$, $[y]$, and $[z]$ denote the major contributions to the nuclear excitations from the corresponding one-dimensional components of the basis functions and are marked in Fig. 8. The calculated transition energies and the Franck–Condon factors for the anthracene·He_1 cluster are in very good agreement with experiment [Fig. 8(a)]. The calculated spectra (relative to the 0–0 origin) are 8.8 $cm^{-1}[y]$, 22.8 $cm^{-1}[y]$, 24.5 $cm^{-1}[x]$, 37.4 $cm^{-1}[y]$, and 49.0 $cm^{-1}[z]$. We assigned the experimental spectra[50] as 8.3 $cm^{-1}[y]$, 23.2 $cm^{-1}[y]$, and 37.3 $cm^{-1}[y]$ [Fig. 8(a)]. The gross features of the vibronic $S_0 \rightarrow S_1$ spectra of the larger anthracene·He_n ($n=2-4$) clusters [Figs. 8(b), 8(c), and 8(d)] are in qualitative agreement with the experimental spectra,[49,50] and the main strong spectral features can be assigned. The calculated lowest vibrationsl $[y]$ excitation of the (2|0) configuration of An·He_2 is at 15.6 cm^{-1}, being considerably higher than the corresponding lowest $[y]$ excitation of An·He_1(8.8 cm^{-1}). This marked difference reflects on the effect of He–He repulsion on the vibrational level structure. The first vibrational excitation of the (2|0) configuration (experimentally observed at 22.8 and 22.3 cm^{-1} for An·He_3 and An·He_4, respectively) is indeed considerably higher in energy than the first vibrational excitation of An·He_1(8.3 cm^{-1}). However, this first vibrational excitation ($\sim$22.5 cm^{-1}) is somewhat higher than the calculated energy (15.6 cm^{-1}) of the (2|0) configuration. There is one notable discrepancy in the confrontation between our theoretical calculations and experimental reality. The spectral feature at 16.5 cm^{-1} experimentally observed for the $n=2$ cluster [Fig. 8(b)], which we attribute to the two-sided $[(1|0)+(0|1)]$ configuration, cannot be assigned by the theoretical calculations. This discrepancy calls for further work transcendenting the approximation of one-sided anthracene·He_2 configurations, while large amplitude nonrigid motion in excited vibrational states can result in overside crossing and nuclear tunneling of the He atom.

IV. CONCLUDING REMARKS

Our study of anthracene·He_n ($n=1,2$) clusters reveals extensive spatial delocalization of the He atoms in the ground vibrational state, both in the S_0 and S_1 electronic states. The spatial delocalization of He on anthracene is highly anisotropic. The delocalization in the *z* and *x* directions (Table II) is confined by the perpendicular restoring force of the aromatic frame and by the horizontal nuclear framework of a single aromatic ring and only weakly depends on small changes in C–He repulsion in the S_1 state and on the strong He–He repulsion. This extent of vertical (*z*) and horizontal spatial delocalization is expected to prevail also for He motion in a single aromatic ring of benzene[36,37] or cyclopentadienyl,[51] for which high resolution spectroscopy can be analyzed in terms of ''apparent rigidity'' of the (floppy) ''small'' clusters.[63] The interesting notion of near complete localization of the two He atoms above and below the benzene ring in benzene·He_{39} inferred by Kwon and Whaley[52] is not expected to apply for large aromatic molecules like anthracene.

The large 1D anisotropic spatial delocalization of He atoms along the *y* axis of anthracene·He_n clusters (Table II) brings up the details of the nonrigidity[64] of these systems in their ground vibrational states. Two elements of the enhancement of the 1D spatial delocalization involve (i) the modification of the He–aromatic molecule repulsive interaction by the electronic $S_0 \rightarrow S_1$ excitation of the microsurface, and (ii) the role of He–He repulsive interaction in spreading the nuclear density across the long, in-plane molecular axis. Regarding the implications of He–He interactions, it should be noted that the description of the He–He interactions involves both He–He repulsion on boson permutational symmetry effects. Further exploration of the consequences of permutation symmetry will be conducted by CI studies of anthracene·$(^3He)_2$ clusters. All large aromatic hydrocarbons are expected to induce anisotropic delocalization. The details of the spatial anisotropic delocalization in aromatic molecule·$(^4He)_n$ clusters will depend crucially on the geometry and the topology of the aromatic microsurface. Linear, long aromatic hydrocarbons, i.e., anthracene, tetracene, and pentacene will exhibit 1D spatial delocalization, while ''circular'' aromatics, e.g., pyrene, perylene or ovalene will ex-

hibit 2D spatial delocalization of He atoms, which is expected to be enhanced by He–He repulsion, calling for further theoretical and experimental studies. The spectral shifts of the electronic origin of the $S_0 \rightarrow S_1$ transition in nonrigid anthracene$\cdot$He$_n$ clusters ($n=1-4$) arise from mutually canceling dispersive (red) and repulsive (blue) contributions, which result in very small overall (red) spectral shifts for the $n=1(1|0)$ and $n=2(1|1)$ clusters. The abrupt increase of the red spectral shifts for $n=3$ and $n=4$ manifests the consequences of the nuclear dynamics of two He atoms on one side of the aromatic microsurface, which involve the large scale nuclear motion (both in the S_0 and S_1 states) and the enhanced 1D delocalization in the S_1 state of these floppy clusters.

The vibrational level structure of the anthracene$\cdot$He$_n$ ($n=1-4$) clusters provides information on the energetics of the quantum states for the large amplitude nonrigid motion in the $(1|0)$ and $(2|0)$ configuration in the S_1 electronic states where 1D spatial delocalization is extensive. The good accord between the calculated energetics and, in particular, the Franck–Condon factors for the $n=1(1|0)$ cluster [Fig. 8(a)] inspires confidence in our description of the nuclear dynamics in these nonrigid systems. On the other hand, a discrepancy was documented in Sec. III C between theoretical and experimental details of the $S_0(1A_1) \rightarrow S_1(nA_1)$ vibronic spectra. This involves the excess experimental spectral feature at 16.5 cm^{-1} for the $n=2$ cluster [Fig. 8(b)]. This sin of excess indicates that the additivity rules,[35] which were invoked for the experimental assignment and the theoretical description of the anthracene$\cdot$He$_n$($n=1-4$) spectra, may not strictly apply for the vibronic level structure. In contrast, the experimental $S_0 \rightarrow S_1$ spectra of tetracene$\cdot$He$_n$ reported by Even and Al-Hroub[50] reveal that the spectra of the $n=1$ and $n=2$ clusters, which can be assigned to the $(1|0)$ and $(1|1)$ configurations, respectively, exhibit the spectral shifts of their origins with $\delta\nu_2 = 2\,\delta\nu_1$, and reveal an identical vibronic level structure, in accord with the additivity rules. Further exploration of the onset of the breakdown of the additivity rules in these M$\cdot$He$_n$ clusters will be informative. It is also possible that, in view of the enhancement of delocalization of the He atoms in excited vibrational states,[48] the additivity rules will be applicable for the electronic origin, while in excited vibrational states deviations from additivity, due to surface crossing, may occur.

The nature and spectra of ''isomeric species'' in aromatic molecule$\cdot$(^{4}He)$_n$ clusters may be relevant for paving the way towards the understanding of collective excitations of ^{4}He atoms confined on a large aromatic molecule and of the solvation of aromatic molecules in superfluid ^{4}He clusters.[31] Of course, the notion of these ''isomeric species'' does not rely on traditional concepts of stereochemistry for isomers in rigid molecular structures, but rather are identified as $(1|0)$ or $(2|0)$ configurations of nonrigid systems, which are subjected to permutation symmetry of identical particles for $n>1$, Toennies *et al.*[31] reported a splitting ($\sim$1 cm^{-1}) of the electronic origin of the $S_0 \rightarrow S_1$ transition of tetracene in large (^{4}He)$_n$ ($n=5000$) clusters, which was tentatively assigned to some ''isomeric species'' (or rather distinct ''configurations''). The theoretical description of the $S_0 \rightarrow S_1$ spectra of anthracene$\cdot$(^{4}He)$_n$($n=1-4$) clusters spectra presented herein, reveals that the lowest excitations are exhibited at 9 cm^{-1} above the electronic origin. Furthermore, the spectral splitting between the electronic origins of An$\cdot$He$_n$ isomer structures, e.g., $n=2(1|1)$ and $(2|0)$, are large $\sim$8 cm^{-1}. The experimental $S_0 \rightarrow S_1$ spectra of tetracene$\cdot$He$_n$($n=1-10$) at 0.4 K (Ref. 50) do also not reveal any small splitting ($\sim$1 cm^{-1}) of the electronic origin. Accordingly, the spectroscopic implications of microscopic solvation of large aromatic molecules in superfluid ^{4}He droplets[31] cannot be accounted for in terms of the spectral features (vibronic structure or isomer splitting) of the corresponding small clusters and require further exploration.

ACKNOWLEDGMENTS

The authors are grateful to Ibrahim Al-Hroub for stimulating discussions. The authors are indebted to the Inter University Computation Center (IUCC) for granting computation time and for excellent service. This research was supported by the German–Israeli James Franck program on laser–matter interactions.

[1] *Molecular Clusters*, edited by E. W. Schlag, R. Weinkauf, and R. E. Miller, Chem. Phys. **239**, 1 (1998).
[2] *Structure and Dynamics of Clusters*, edited by T. Kondow, K. Kaya, and A. Terasaki (University Press, Tokyo, 1996).
[3] *Small Particles and Inorganic Clusters (ISSP 9)*, edited by J. M. Bonard and A. Chatelin (Springer-Verlag, Berlin, 1999).
[4] J. Jortner, Z. Phys. D: At., Mol. Clusters **24**, 247 (1992).
[5] P. Alivisatos, Science **271**, 933 (1996).
[6] S. C. Pieper, R. B. Wiringa, and V. R. Pandharipande, Phys. Rev. B **32**, 3341 (1985).
[7] V. R. Pandharipande, S. C. Pieper, and R. B. Wiringa, Phys. Rev. B **34**, 4571 (1986).
[8] M. V. Rama Krishna and K. B. Whaley, J. Chem. Phys. **93**, 6738 (1990).
[9] S. Stringari and J. Treiner, J. Chem. Phys. **87**, 5021 (1987).
[10] D. M. Brink and S. Stringari, Z. Phys. D: At., Mol. Clusters **15**, 257 (1990).
[11] S. A. Chin and E. Krotscheck, Phys. Rev. B **45**, 852 (1992).
[12] M. V. Rama Krishna and K. B. Whaley, Mod. Phys. Lett. B **4**, 895 (1990).
[13] M. Casas, F. Dalfovo, A. Lastri, Ll. Serra, and S. Stringari, Z. Phys. D: At., Mol. Clusters **35**, 67 (1995).
[14] M. Casas and S. Stringari, J. Low Temp. Phys. **79**, 135 (1990).
[15] E. Cheng, M. A. McMahon, and K. B. Whaley, J. Chem. Phys. **104**, 2669 (1996).
[16] M. A. McMahon and K. B. Whaley, J. Chem. Phys. **103**, 2561 (1995).
[17] M. A. McMahon, R. N. Barnett, and K. B. Whaley, Z. Phys. B: Condens. Matter **98**, 421 (1995).
[18] P. Sindzingre, M. L. Klein, and C. M. Ceperley, Phys. Rev. Lett. **63**, 1601 (1989).
[19] L. Pitaevskii and S. Stringari, Z. Phys. D: At., Mol. Clusters **16**, 299 (1990).
[20] J. P. Toennies and A. F. Vilesov, Annu. Rev. Phys. Chem. **49**, 1 (1998).
[21] M. Hartmann, F. Mielke, J. P. Toennies, A. F. Vilesov, and G. Benedek, Phys. Rev. Lett. **76**, 4560 (1996).
[22] M. Farnik, U. Henne, B. Samelin, and J. P. Toennies, Phys. Rev. Lett. **81**, 3892 (1998).
[23] S. Grebenev, J. P. Toennies, and A. F. Vilesov, Science **279**, 2083 (1998).
[24] S. Grebenev, M. Hartmann, M. Havenith, B. Sartakov, J. P. Toennies, and A. F. Vilesov, J. Chem. Phys. **112**, 4485 (2000).
[25] M. Hartmann, R. E. Miller, J. P. Toennies, and A. Vilesov, Phys. Rev. Lett. **75**, 1566 (1995).
[26] K. Nauta and R. E. Miller, Phys. Rev. Lett. **82**, 4480 (1999).
[27] C. Callegari, A. Conjusteau, I. Reinhard, K. K. Lehmann, G. Scoles, and F. Dalfovo, Phys. Rev. Lett. **83**, 5058 (1999).
[28] Y. Kwon and K. B. Whaley, Phys. Rev. Lett. **83**, 4108 (1999).
[29] Y. Kwon, P. Huang, M. Patel, D. Blume, and K. B. Whaley, J. Chem. Phys. **113**, 6469 (2000).

[30] K. Nauta, D. T. Moore, and R. E. Miller, Faraday Discuss. **113**, 261 (1999).
[31] M. Hartmann, A. Lindinger, J. P. Toennies, and A. F. Vilesov, Chem. Phys. **239**, 139 (1998).
[32] A. Amirav, U. Even, and J. Jortner, Chem. Phys. Lett. **67**, 9 (1979).
[33] S. Leutwyler and J. Jortner, J. Phys. Chem. **91**, 5558 (1987).
[34] E. Shalev, N. Ben-Horin, and J. Jortner, Chem. Phys. Lett. **177**, 161 (1991).
[35] E. Shalev, N. Ben-Horin, U. Even, and J. Jortner, J. Chem. Phys. **95**, 3147 (1991).
[36] R. E. Smalley, L. Wharton, D. H. Levy, and D. W. Chandler, J. Chem. Phys. **68**, 2487 (1978).
[37] S. M. Beck, M. G. Liverman, D. L. Monts, and R. E. Smalley, J. Chem. Phys. **70**, 232 (1979).
[38] D. H. Levy, C. A. Haynam, and D. V. Brumbaugh, Faraday Discuss. **73**, 137 (1982).
[39] T. S. Zwier, E. Carrasquillo, and D. H. Levy, J. Chem. Phys. **78**, 5493 (1983).
[40] C. A. Haynam, D. V. Brumbaugh, and D. H. Levy, J. Chem. Phys. **80**, 2256 (1984).
[41] E. R. Bernstein, K. Law, and M. Schauer, J. Chem. Phys. **80**, 634 (1984).
[42] C. A. Taatjes, W. B. Bosma, and T. S. Zwier, Chem. Phys. Lett. **128**, 127 (1986).
[43] K. Yamanouchi, S. Isogai, and S. Tsuchiya, Chem. Phys. **116**, 123 (1987).
[44] D. O. DeHaan, A. L. Holton, and T. S. Zwier, J. Chem. Phys. **90**, 3952 (1989).
[45] T. S. Zwier, J. Chem. Phys. **90**, 3967 (1989).
[46] D. H. Semmes, J. S. Baskin, and A. H. Zewail, J. Chem. Phys. **92**, 3359 (1990).
[47] B. Coutant and P. Bréchignac, J. Chem. Phys. **100**, 7087 (1994).
[48] A. Bach, S. Leutwyler, D. Sabo, and Z. Bacic, J. Chem. Phys. **107**, 8781 (1997).
[49] U. Even, J. Jortner, D. Noy, N. Lavie, and C. Cossart-Magos, J. Chem. Phys. **112**, 8068 (2000).
[50] I. Al-Hroub, U. Even, and J. Jortner, J. Chem. Phys. **115**, 2069 (2001).
[51] L. Yu, J. Williamson, S. C. Foster, and T. A. Miller, J. Chem. Phys. **97**, 5273 (1992).
[52] Y. Kwon and K. B. Whaley, J. Chem. Phys. **114**, 3163 (2000).
[53] K. F. Lim, J. Chem. Phys. **101**, 8756 (1994).
[54] G. Vidali, M. W. Cole, and W. H. Weinberg, Phys. Rev. Lett. **51**, 118 (1983).
[55] W. E. Carlos and M. W. Cole, Surf. Sci. **91**, 339 (1980).
[56] G. Scoles, Annu. Rev. Phys. Chem. **31**, 81 (1980).
[57] J. P. Toennies, W. Welz, and G. Wolf, Chem. Phys. Lett. **44**, 5 (1976).
[58] A. Heidenreich, I. Last, U. Even, and J. Jortner, Phys. Chem. Chem. Phys. **3**, 2325 (2001).
[59] *CRC Handbook of Chemistry and Physics*, 62nd ed. (CRC, Boca Raton, FL, 1981).
[60] R. J. Vos, J. H. van Lenthe, and F. B. van Duijnenveldt, J. Chem. Phys. **93**, 643 (1990).
[61] D. M. Ceperley and H. Partridge, J. Chem. Phys. **84**, 820 (1986).
[62] R. A. Aziz and M. J. Slaman, J. Chem. Phys. **94**, 8047 (1991).
[63] D. J. Nesbitt and R. Naaman, J. Chem. Phys. **91**, 3801 (1989).
[64] R. S. Berry, in *Quantum Dynamics of Molecules*, edited by R. G. Wooley (Plenum, New York, 1980), p. 143.